

GrapheneBased Pressure Sensor Application in NonInvasive Pulse Wave Velocity Continuous Estimation

Original

GrapheneBased Pressure Sensor Application in NonInvasive Pulse Wave Velocity Continuous Estimation / Buraioli, I., Vitale, S., Valerio, A., Sanginario, A., Leone, D., Conoci, S., Ciesielski, A., Milan, A., Demarchi, D., Samori, P.. - In: ADVANCED MATERIALS TECHNOLOGIES. - ISSN 2365-709X. - 10:5(2025). [10.1002/admt.202400876]

Availability:

This version is available at: 11583/3002463 since: 2025-08-19T14:06:12Z

Publisher:

Wiley

Published

DOI:10.1002/admt.202400876

Terms of use:

This article is made available under terms and conditions as specified in the corresponding bibliographic description in the repository

Publisher copyright

(Article begins on next page)

Graphene-Based Pressure Sensor Application in Non-Invasive Pulse Wave Velocity Continuous Estimation

Irene Buraioli,* Stefania Vitale, Andrea Valerio, Alessandro Sanginario, Dario Leone, Sabrina Conoci, Artur Ciesielski, Alberto Milan, Danilo Demarchi, and Paolo Samori*

Monitoring the cardiovascular health of patients and early diagnosis of heart diseases are highly sought after as they can represent a true cornerstone in tomorrow's healthcare surveillance. Here, an unprecedented non-invasive device prototype is reported for pulse wave velocity (PWV) measurement based on a piezoelectric graphene pressure sensor. PWV is a critical health indicator that estimates arterial stiffness by measuring the velocity of arterial pulse flow through the circulatory system. The sensor incorporates advanced electronic components and data analysis tools, enabling the measurement of pulse transit time (PTT), that is the time required for the pulse wave to travel between carotid and femoral artery sites. Significantly, the outcomes obtained through the novel method, which involved monitoring 10 patients within clinical environment, show statistical similarity to results obtained using established technology for the PWV estimation such as SphygmoCor. In particular, the mean difference between measurements done with the two techniques resulted in 0.1 m s^{-1} , that is $<2\%$, underscoring the reliability of the novel device. The technology holds big promise for enhancing cardiovascular healthcare delivery: it is wearable, potentially exploitable by a non-expert user, and it needs to be powered with just 0.2 V, thus it can become compatible even with applications in point-of-care settings.

year.^[1] Therefore, the development of advanced heart monitoring tools capable of swift and accurate diagnosis, potentially operating in point-of-care settings, is highly demanded. Among the multifaceted factors of cardiovascular disorders, arterial stiffness emerges as a major cause, instigating pervasive organ damage and untimely fatalities such as heart attacks and strokes.^[2,3] Over the past few years, clinical assessment of pulse wave velocity (PWV) has been proposed and demonstrated being a powerful, non-invasive method for physiological parameters and cardiovascular analysis. The evaluation is done by measuring the velocity at which arterial pulse flows through the circular system,^[4] which is related to arterial stiffness and compliance. This new approach holds the important promise of revolutionizing cardiovascular assessment by offering a transformative paradigm shift toward proactive and personalized patient management, ultimately saving countless

1. Introduction

Cardiovascular diseases represent nowadays the leading cause of mortality in our planet, with over 17.9 million deaths each

lives, and mitigating the burden of cardiovascular disease worldwide. The PWV estimation involves determining the pulse's transit time between specific points, typically the carotid and femoral artery sites.^[5–7] Pulse Transit Time (PTT) is the exact

I. Buraioli, A. Valerio, A. Sanginario, D. Demarchi
Department of Electronics and Telecommunications
Corso Duca Degli Abruzzi 24, Politecnico di Torino, Torino 10129, Italy
E-mail: irene.buraioli@polito.it
S. Vitale, A. Ciesielski, P. Samori
University of Strasbourg
CNRS
Institut de Science et d'Ingénierie Supramoléculaires
UMR 7006, 8 Allée Gaspard Monge, Strasbourg 67000, France
E-mail: samori@unistra.fr

D. Leone, A. Milan
Candiolo Cancer Institute FPO-IRCCS
Division of Internal Medicine
Department of Medical Science University of Turin
Candiolo (TO) 10060, Italy
S. Conoci
Department of Chemical, Biological, Pharmaceutical and Environmental
Sciences (ChiBioFarAm)
University of Messina
Viale F. Stagno d'Alcontres 31, Messina 98166, Italy
S. Conoci
LAB Sense Beyond Nano – URT Department of Sciences Physics and
Technologies of Matter
Consiglio Nazionale delle Ricerche (CNR-DSFTM)
Viale F. Stagno d'Alcontres 31, Messina 98166, Italy
S. Conoci
Department of Chemistry "G. Ciamician"
University of Bologna
Via F. Selmi 2, Bologna 40126, Italy

 The ORCID identification number(s) for the author(s) of this article can be found under <https://doi.org/10.1002/admt.202400876>

© 2024 The Author(s). Advanced Materials Technologies published by Wiley-VCH GmbH. This is an open access article under the terms of the [Creative Commons Attribution](https://creativecommons.org/licenses/by/4.0/) License, which permits use, distribution and reproduction in any medium, provided the original work is properly cited.

DOI: 10.1002/admt.202400876

time required for the pulse wave to travel this distance, which is known as Pulse Wave Distance (PWD). The ratio between these two values represents the propagation velocity of the wave.^[8] For healthy adults, the reference value for PWV is $\approx 6 \text{ m s}^{-1}$.^[9] However, this value tends to increase with age and the presence of additional health complications, such as diabetes, reaching values $\approx 9 \text{ m s}^{-1}$. According to the most recent recommendations from the European Society of Hypertension, in middle-aged patients with hypertension, a measured PWV exceeding 10 m s^{-1} may indicate significant alterations in aortic function.^[10] Therefore, reliable PWV values obtained from asymptomatic patients could facilitate early assessment of arterial stiffness, leading to more accurate estimations of cardiovascular risk and enabling timely therapy targeting.^[10] Several technologies have been developed and exploited for the non-invasive PWV evaluation.^[11,12] Applanation tonometry is the most extensively utilized approach to detect the pressure wave generated by the systolic ejection of the heart at two distinct locations, with the SphygmoCor (AtCor Medical, Sydney, Australia) being the most widely used tool for PWV evaluation in clinical environments.^[13] Less commonly employed techniques include piezoelectric mechanotransducers, cuff-based oscillometry, ultrasounds, and photoplethysmography.^[14,15] Besides their high costs, each of these techniques necessitates skilled operators to conduct the measurements. Consequently, the widespread adoption of PWV assessment in clinical practice and beyond faces obstacles due to these requirements.

Physical sensing devices stand as pivotal components within the realm of smart wearable electronics, with pressure and strain sensors emerging in view of their high technological relevance in motion detection, health monitoring, robotics, human-machine interaction, electronic skin, and Internet of (Medical) Things, etc.^[16] Recent progress in pressure and strain sensing has led to significant enhancements in device performance, notably by elevating the relevant key performance indicators such as sensitivity, detectable pressure range, response speed, and cyclability. The unique properties of flexible pressure sensors, including conformability and high sensitivity, render them exceptionally well-suited for monitoring physiological parameters and detecting health conditions.^[17,18] Through their integration into wearable devices or smart fabrics, the unobtrusive long-term monitoring of vital signs, such as heartbeat,^[19,20] physiological pressure,^[21,22] respiratory rate,^[23,24] and human motion^[18,19] becomes achievable. This integration facilitates the provision of real-time feedback to the end user, thereby enhancing their ability to monitor and manage their health effectively.^[25]

Recently, some of us developed a graphene-based piezoresistive pressure sensor, which holds significant promise for health monitoring applications.^[26] Such device is composed of a spray-coated multi-layered film of reduced graphene oxide functionalized with flexible triethylene glycol chains (frGO), sandwiched between two indium tin oxide (ITO)-coated polyethylene terephthalate (PET) electrodes. The application of external pressure decreases the device's electrical resistance, which is ruled by electron tunnelling between adjacent frGO sheets. Such pressure sensor exhibits exceptional performance in terms of sensitivity (up to 0.82 kPa^{-1}), response time (24 ms), detection limit (7 Pa), and durability (over 1000 cycles),^[26] making it highly suitable as

a component for its integration in a new generation of PWV technologies.

In this study, we demonstrate how this frGO-based pressure sensor can be integrated as suitable detection element in a prototypical clinical device for Pulse Wave Velocity assessment. Tests were conducted by specialized physicians on ten healthy volunteers. First, the sensors were placed on selected carotid and femoral sites, and then the pulses were acquired using a customized electronic system. The operators could check the quality of the detected pulse waves in real time through a dedicated graphical user interface (GUI), which displays the waves. To assess the precision and reliability of our device, the estimated values were benchmarked against those measured with the golden standard, that is, SphygmoCor.

2. Results and Discussion

2.1. Graphene-Bases Sensors Preparation and Integration

The chemically functionalized reduced graphene oxide (rGO) active material (called frGO hereafter) was prepared by following a procedure previously developed and reported by some of us,^[26] whose details are presented in Section S1 (Supporting Information). The solution-based rGO functionalization protocol that we developed allows for precise control of the active material properties through incorporation of a flexible linker (triethylene glycol amine), resulting in a solution processable material, compatible with most used flexible substrates and with spraying and printing deposition techniques, with potential for implementation at industrial level. The final material consisted in a homogeneous dispersion of rGO functionalized with triethylene glycol amine in ethanol. Such dispersion was then used to fabricate our graphene-based pressure sensing devices according to our reported literature procedures presented in Section S2 (Supporting Information).^[26,27]

The final device consists of two frGO-coated electrodes assembled in a face-to-face configuration, fixed together by polyimide tape. The tape also has the function of sealing the device, thus preventing potential interference of air and humidity. Electrical contacts were made by fixing copper wires with silver paste (see S3 Section, Supporting Information, for details). **Figure 1** portrays a scheme of the prepared pressure sensors and their piezoresistive working mechanism, whereas their piezoresistive behavior characterization is reported in (Figure S4.1, Supporting Information).

The sensors' performance was evaluated in terms of pressure sensitivity and device robustness upon application of cyclic stress (Figure S4.1, Supporting Information). In the present work, the static pressure and durability tests carried out on the prepared devices confirmed high sensitivity of 0.77 kPa^{-1} in the low-pressure regime (up to 0.6 kPa), a fast response time of 25 ms, and good stability upon cycles, as quantified by only 10% performance loss after 1000 load-unload cycles.

2.2. Integration

The prepared frGO-based pressure sensors were subsequently embedded into customized holders which have been designed

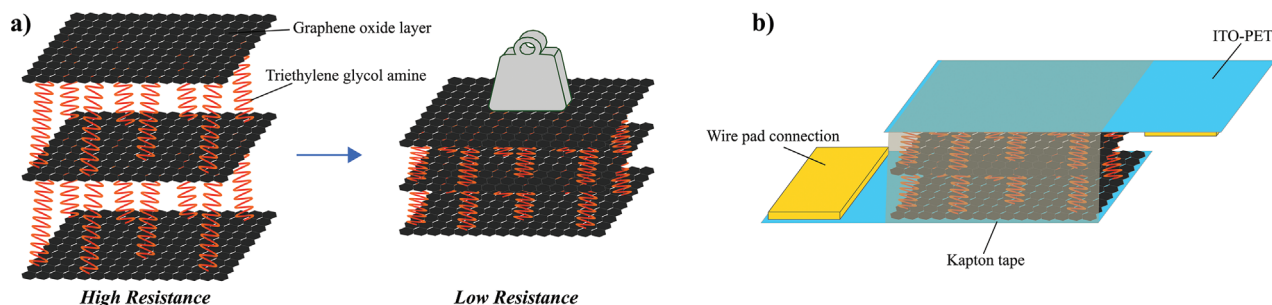


Figure 1. Functionalized graphene-based pressure sensors: a) scheme of the working mechanism, b) final configuration of the device, with pads for wires connection.

to enable the sensor's integration on two elastic bands and perform the PWV assessment. The latter renders the sensor wearable without requiring the constant presence of an operator to hold them on the pulse sites, thereby optimizing the signal acquisition and the device operation.

The signals detected by the two sensors, immobilized at the femoral and carotid sites, are then synchronously processed by an acquisition board, developed specifically for this application, which is also responsible for sending data to a working station. In addition, a graphical user interface (GUI) allows real-time signal visualization, giving the opportunity to the operator to replace the

sensors in case the data are not matching the required quality. **Figure 2** provides an overview of the system.

2.3. Sensor Engineering and Electronics Read-Out

To guarantee optimal sensor's engineering, one should consider that changes in the resistance detected by the graphene sensor must be proportional to the variation in the applied transverse pressure. Thus, the precise detection of the vital signal requires the sensor immobilization on the skin. This was accomplished by

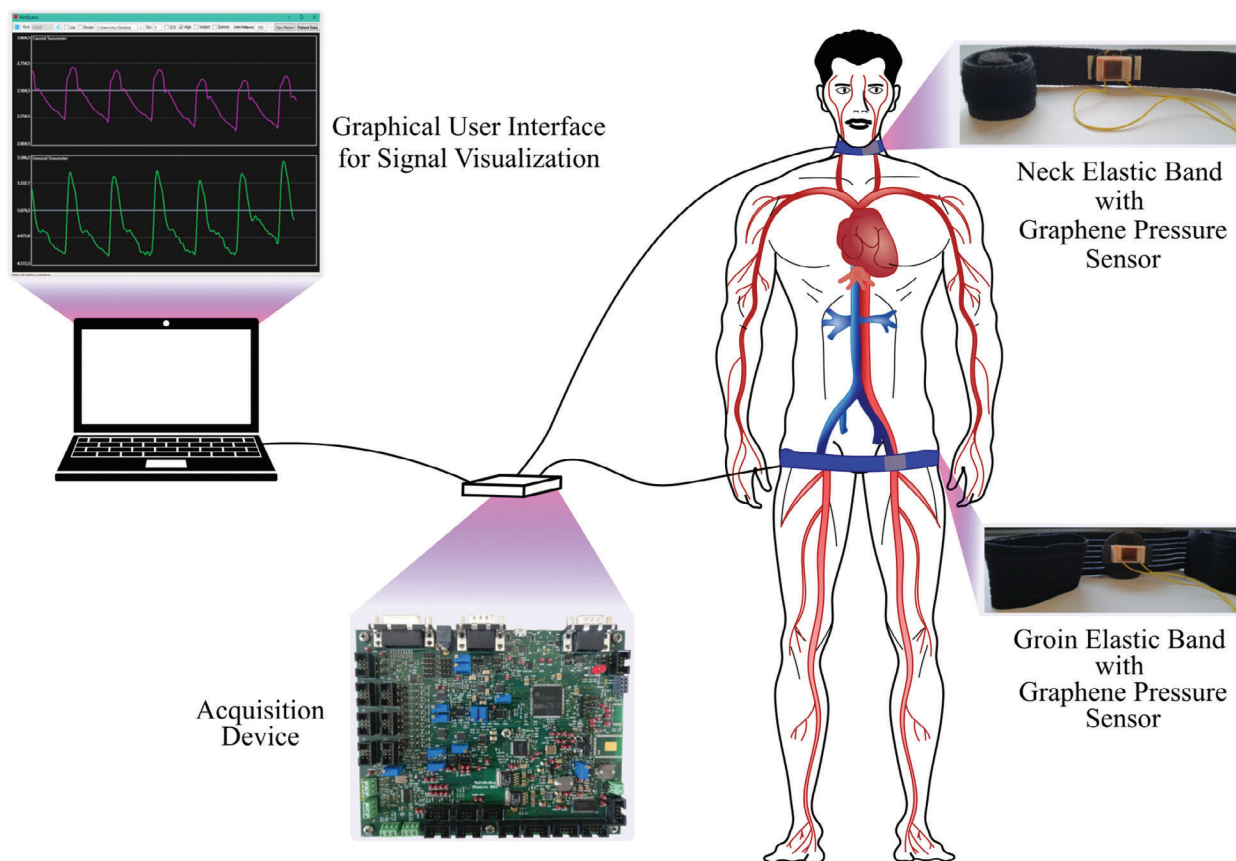


Figure 2. Overview of the system comprising the two graphene pressure sensors supported by an elastic band (one for the carotid signal on the neck, and the other for the femoral in the groin), the electronic board for signal acquisition and process, and a processing unit for data visualization, storage and PWV evaluation.

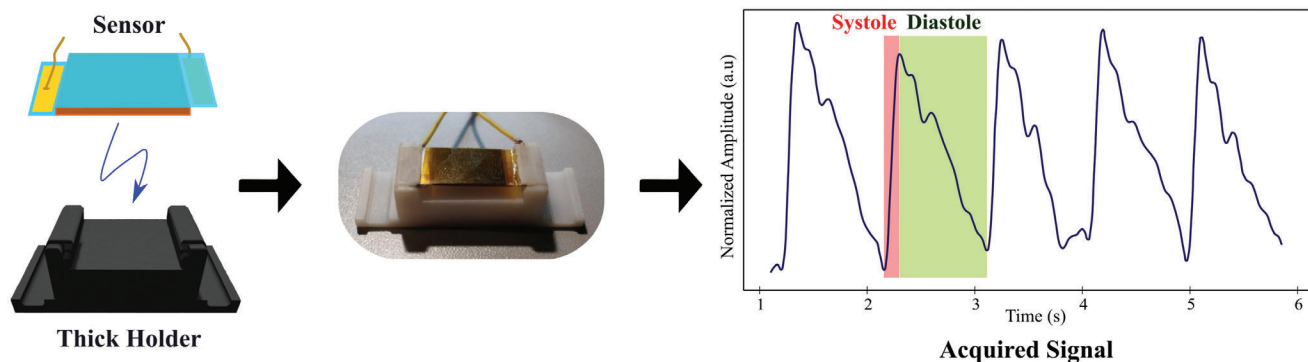


Figure 3. Sensor engineering. The graphene sensor is embedded in a 3D-printed thick holder to be readily positioned in proximity of an artery (carotid) and used to record the pulse wave with a high precision.

custom manufacturing a 3D-printed support such as the “Thick Holder” in **Figure 3**, which clamps the sensor and fastens it to a band, thus improving wearability and preventing its rubbing. The holder shape and 3D structure were carefully tailored by following an iterative improvement process (reported in Supporting Information) that tested different sensor engineering strategies against their performance. The holder’s thickness (≈ 7 mm) amplifies the static pressure applied by the band, enabling the detection of minor dynamic fluctuations and facilitating the recording of heartbeats at increased depth (as detailed in Section S5 of the Supporting Information). The holder is specifically designed to aid in positioning the sensor at the acquisition site without compromising its performance. Moreover, it enables longer signal acquisition periods. The combination of the belt and holder allows

the sensor to remain securely positioned for long-term data collection without causing pain or discomfort to the subject.

When the sensor is positioned near an arterial site, such as the carotid artery in the neck, it can capture a signal that closely replicates the pulse wave typically detected by conventional methods, such as applanation tonometry. As depicted in **Figure 3**, the acquired signal exhibits a discernible rhythmic pattern characteristic of the heartbeat, wherein each cycle comprises two distinct phases: a rising front, due to the abrupt expansion of the vessel in the first part of the cardiac period (systole), and the slower descending phase (linked with the gradual decreasing pressure occurring in the diastole).

The scheme of the electronic read-out is shown in **Figure 4**. Its design enables efficient and consistent data acquisition, despite

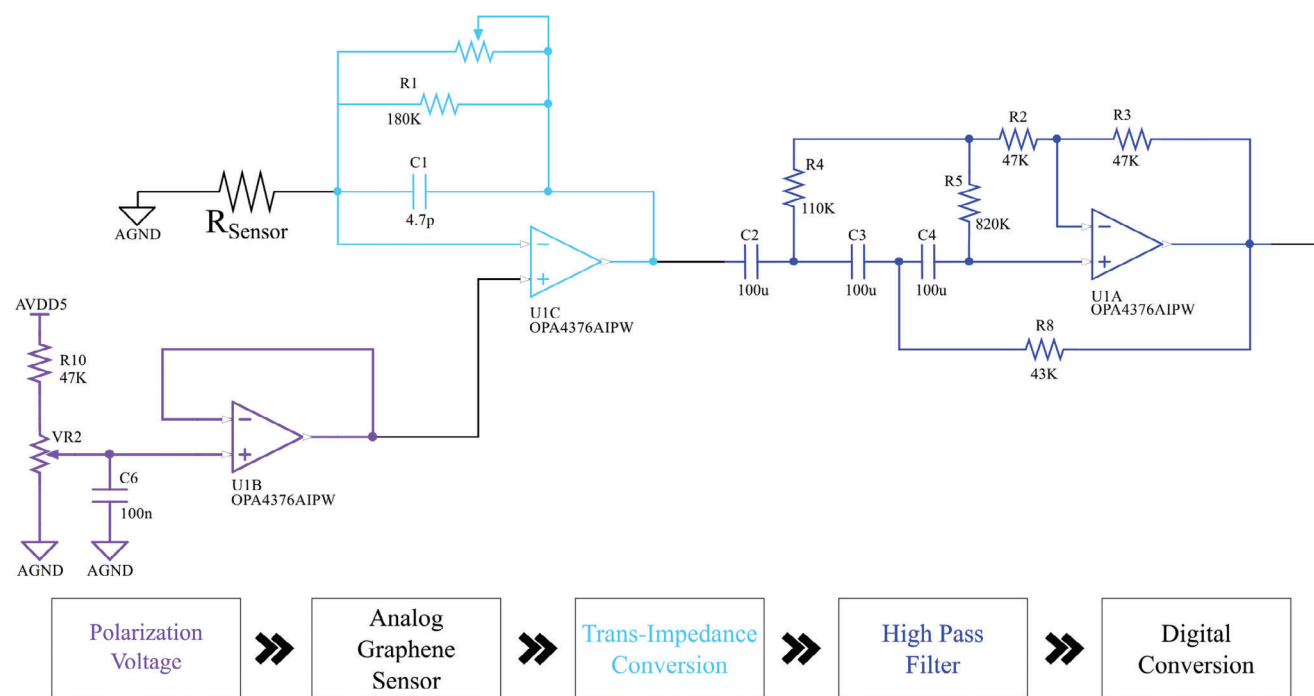


Figure 4. Scheme of the electronics enabling the sensor’s readout. It comprises the current reading (purple), the trans-impedance amplifier (light green), and second order filter (blue) to accomplish digital conversion.

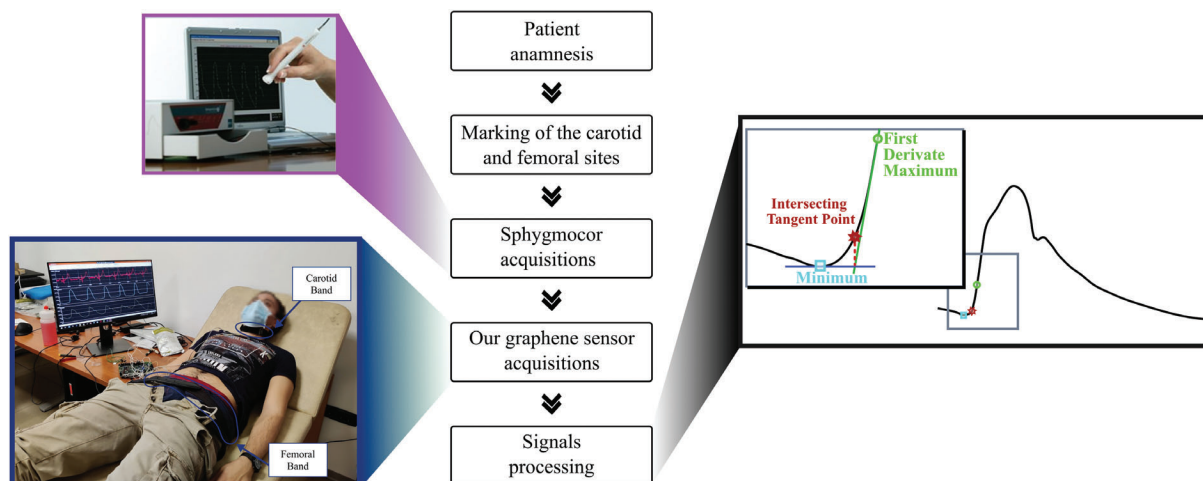


Figure 5. Validation study flow chart and protocol for each tested subject comprising sub-sequentially the patient anamnesis, the data acquisition, and the signal processing. The latter is used to extract the Intersecting Tangent Point.

the variability in resistance baseline values (which change from sensor to sensor) and the different static pressures applied by the elastic bands (which depend on the subject physiology).

The electronics comprises three major elements. The first is the sensor biasing block in which the appropriate voltage is generated, stabilized by the voltage follower (U1B Operation Amplifier, OPA), and then applied to the sensor owing to the U1C inputs mirroring properties. Such a block enables the measurement of the sensor baseline resistance by targeting currents of some mA flowing in the sensor, with the voltage value being set through the potentiometer VR2. The second element converts the variation of current in voltage by the U1C trans-impedance amplifier. A potentiometer is placed in the negative feedback to manually adjust the channel's gain while acquiring the data. The third op-amp is a second-order high-pass filter with a cut-off frequency of 0.1 Hz to remove the signal continuous component (offset) and stabilize the signal. Finally, the wave is digitally converted and sent through USB to a laptop where a GUI, developed in Visual Studio environment, enables the data visualization and storage.

2.4. Clinical Validation and Signal Processing

Our new PWV system has been exploited to monitor ten healthy subjects who simultaneously have undergone PWV clinical testing using the established SphygmoCor technology. Two experienced clinical operators were involved in the data collection procedures to ensure the acquisition of high-quality and stable signals. Ten individuals underwent a set of three acquisitions employing both systems (see Section S6, Supporting Information, for the subjects' anamnestic characteristics). The recording started once the carotid and femoral signals were considered stable for 30 s, and data were stored for offline processing. All the key steps characterizing the testing of a given patient are summarized in **Figure 5**.

The acquired data were post-processed in Matlab to compute the PWV related to each test. A feature that identifies the ex-

act moment of the wave-passage in the acquisition site was extracted from each pulse. The ad hoc engineering of the support holder and the correct band placement guaranteed signals with a shape comparable to the pulse usually monitored by a tonometer (through a transducer placed in a pen and held by clinicians). Toward this end, we extracted the Intersecting Tangent Point (ITP), which has been extensively reported in the literature for PWV analysis and used by the golden standard, enabling facile benchmarking.^[6] More precisely, the ITP can be singled out focussing on the rising part of the heart wave, by tracing two lines, the former being parallel to the abscissa and passing through the minimum before the rise, and the latter being the tangent to the steepest part of the curve. The projection of their intersection is the Intersecting Tangent Point, known also as “foot of the signal”, representing the timestamp of the wave passage in the acquisition site (see **Figure 5**).

2.5. PWV Assessment on Test Subjects

Figure 6 compares the pulse waves diagrams on a representative subject recorded by the SphygmoCor and by the graphene-based sensor. Despite the major differences in the two techniques, their output is very similar. On the one hand, the golden standard, shown in the left panel, requires a two-step acquisition protocol based on the data collection attained using a physical sensor (black line) combined with the electrocardiogram signal (ECG, blue line). The PWV is computed from the pulse transit time which is determined by subtracting the femoral and the carotid transit time. These two are quantified individually as the time difference between the R-peak of the ECG (green dot on the blue line) and the foot of the pulse (green dot on the black line). On the other hand, our graphene sensor-based device, displayed in the right panel, simultaneously acquires the signals at the carotid and femoral sites, thereby extracting the intersecting tangent points (blue dots). Hence, our novel technology combines two key features: it can capture data in a single step and, most importantly, it does not require the presence of a skilled operator during the

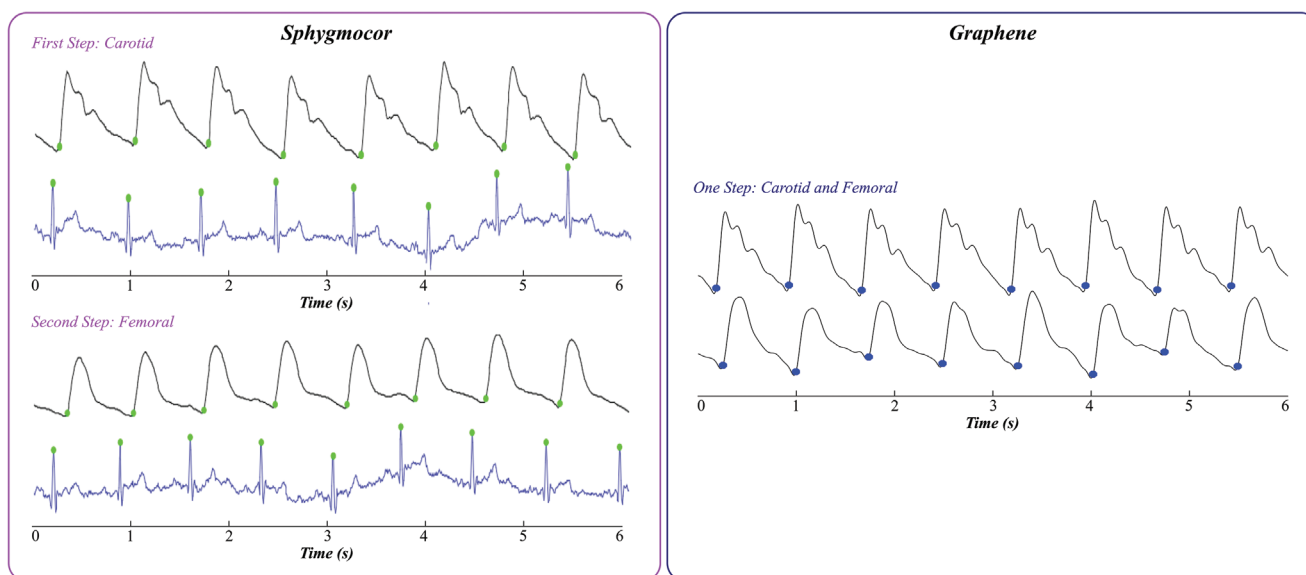


Figure 6. Comparative pulse wave diagrams recorded by means of the SphygmoCor (left), in a two steps acquisition process, and by the graphene-based sensor (right), with the two signals acquired simultaneously.

data acquisition. In fact, following the positioning of the sensors at the neck and groin, the system autonomously proceeds with the signals acquisition.

Table 1 and **Figure 7** report a statistical comparison of the data recorded with the graphene sensor-based device and the golden standard. Each provided value (mean and standard deviation) is the result of an arithmetical average of three acquisitions conducted with the two set-ups. Significantly, when compared to the SphygmoCor, our graphene-based device showed excellent accuracy as quantified by average difference of 0.1 m s^{-1} , which corresponds to $<2\%$. In fact, as outlined by Artery guidelines,^[28] the comparison between the golden standard and a new technology can be classified according to three ranges on the basis of the average difference and its standard deviation: excellent ($\leq 0.5 \pm 0.8 \text{ m s}^{-1}$), acceptable ($< 1 \pm 1.5 \text{ m s}^{-1}$), and poor ($\geq 1 \pm 1.5 \text{ m s}^{-1}$).

The coefficient variation (CV) on the PWVs across all subjects was examined to assess the measurement uncertainty. This pa-

rameter is a dispersion index that expresses the precision and repeatability of a measurement, and it can be quantified using the following formula:

$$CV[\%] = 100 \times \frac{\sigma}{|PWV_{\text{mean}}|} \quad (1)$$

where σ is the standard deviation and $|PWV_{\text{mean}}|$ is the average value of the PWV determined from the three measurements. **Figure 7b** reveals that our graphene-based device consistently displays lower values than the SphygmoCor (3.6% vs 5.4%). This underscores the potential of our device to offer a trustworthy alternative to the gold standard, which, in contrast, exhibits the highest average uncertainty.

A careful analysis of the distribution reveals that significant deviations between the two systems often coincide with greater variability within the measurements. For example, volunteers 6

Table 1. Validation Results.

| Subject ID | PTT _{cf} Sphy [ms] | sd Sphy [ms] | PTT _{cf} Graph [ms] | sd Graph [ms] | Distance [ms] | PWV Sphy [m s ⁻¹] | PWV Graph [m s ⁻¹] | Difference [m s ⁻¹] |
|------------------|--------------------------------|-----------------|---------------------------------|------------------|------------------|----------------------------------|-----------------------------------|------------------------------------|
| 1 | 7220 | 636 | 7205 | 270 | 472 | 65 | 66 | 00 |
| 2 | 6330 | 141 | 7069 | 273 | 496 | 78 | 70 | 08 |
| 3 | 7210 | 113 | 7994 | 290 | 448 | 62 | 56 | 06 |
| 4 | 7435 | 233 | 7222 | 332 | 488 | 66 | 68 | -02 |
| 5 | 8040 | 382 | 7106 | 224 | 480 | 60 | 68 | -08 |
| 6 | 6720 | 679 | 7483 | 382 | 440 | 65 | 59 | 07 |
| 7 | 7705 | 940 | 7075 | 207 | 520 | 67 | 74 | -06 |
| 8 | 8800 | 240 | 8604 | 226 | 440 | 50 | 51 | -01 |
| 9 | 7635 | 276 | 8565 | 045 | 472 | 62 | 55 | 07 |
| 10 | 7525 | 361 | 7498 | 468 | 440 | 58 | 59 | 00 |
| Mean Difference: | | | | | | | | 01 |

Abbreviations: PTT (Pulse Transit Time), sd (standard deviation), Sphy (Sphygmocor system), Graph (Graphene system).

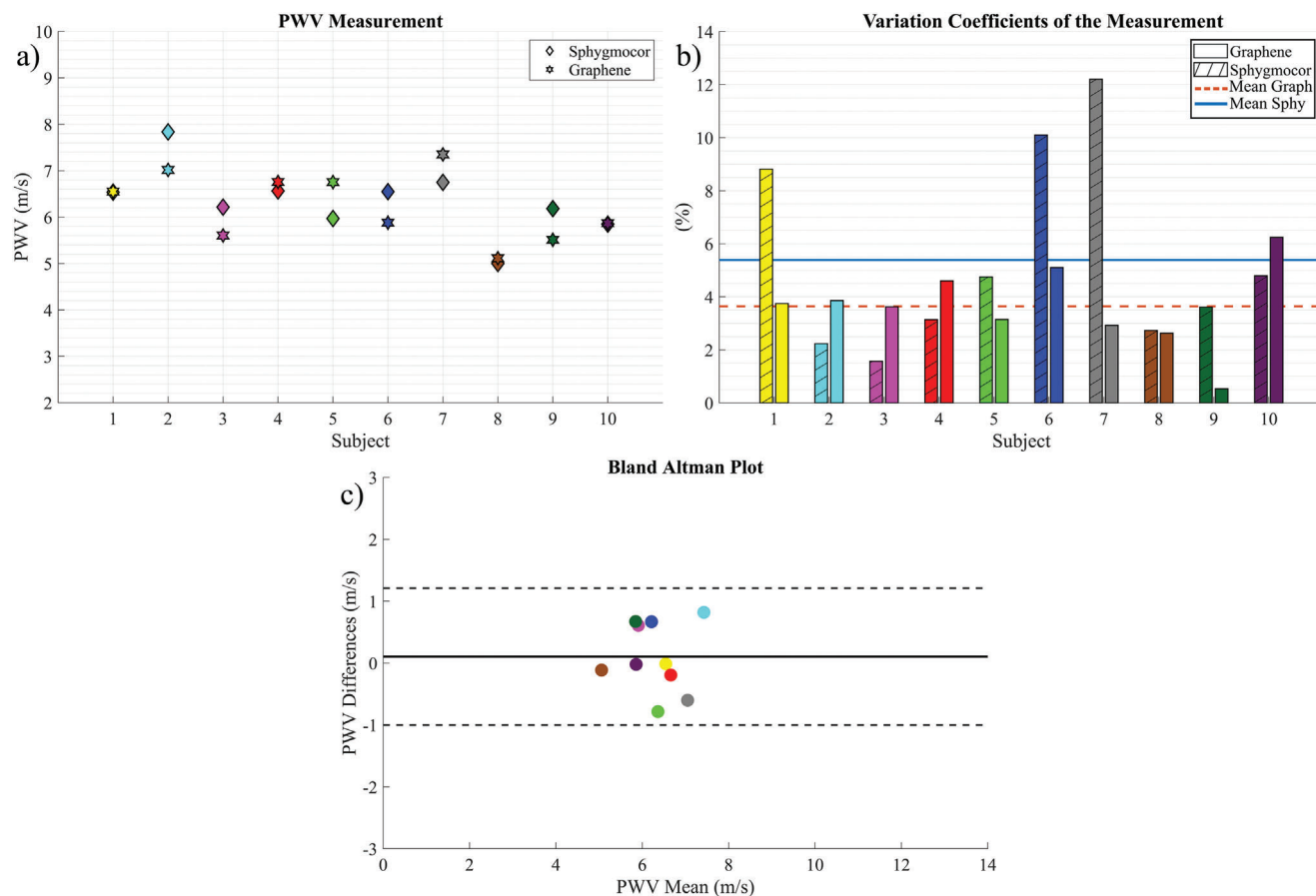


Figure 7. Comparison between the results determined with the two devices for each subject: a) PWV measurements distribution, b) variation coefficients on the measurements, and c) Bland Altman plot.

and 7 display disparities of 0.7 and -0.6 m s^{-1} , respectively, with SphygmoCor exhibiting high standard deviation values (10% and 12%). This emphasizes the good stability and reproducibility of our device measurements.

Table 1 reveals that all estimated PWV values amount to ca. 6 m s^{-1} , confirming that the ten patients under study are in good cardiovascular health and do not suffer from hypertension-related diseases, in line with expectations (details on the patient's physiological parameters such as age and gender are provided in Supporting Information).

Finally, the Bland–Altman Plot (Figure 7c) is used to assess the alignment in output PWV values distribution obtained using the two devices under examination. It reveals an excellent agreement between the two techniques, as evidenced by all data points (corresponding to the differences) falling within the graph area, delimited by the two solid lines representing an acceptable confidence interval. Notably, the maximum deviation observed is $\approx 0.8 \text{ m s}^{-1}$, for one participant, the fifth. Conversely, for four volunteers (1, 4, 8, and 10), the final Pulse Wave Velocity (PWV) measurements exhibit perfect congruence.

These findings collectively provide unambiguous evidence that our approach for Pulse Wave Velocity assessment represents a valid alternative to established technologies yet offering major

advantages in terms of easiness of the measurement (not requiring specialized operator) and portability.

3. Conclusion

We have demonstrated the effective use of graphene-based sensors to record arterial pulse at the carotid and femoral sites, and their integration to estimate the Pulse Wave Velocity with high precision. We attained accurate pulse wave recordings at both the carotid and femoral sites through meticulous optimization of both the holder and electronics. This approach yielded stable signals using a self-contained methodology that achieves signal quality and waveforms comparable to those obtained from established sensors, such as tonometry, while removing the necessity for continuous holding and oversight by a specialized operator. Our methodology enables the continuous monitoring of the PWV for an early assessment of arterial stiffness to ultimately enhance cardiovascular healthcare. The values we obtained revealed robust correlation and similarity to those generated by a commercial device, with an average discrepancy of 0.1 m s^{-1} , that is, $<2\%$. In terms of reliability, our unprecedented technology displays extremely high performance, as evidenced by a mean percentage standard deviation of 3.6%, which is inferior to the 5.4% detected in the traditional golden standard method.

The engineered PWV device is portable and powered by a small voltage (0.2 volts), thus it is energy efficient. Such characteristics make the technology compatible with a point-of-care setting, for remote monitoring even in the absence of a power supply. All in all, our PWV set-up holds potential to become a key component for tomorrow's Internet of Medical Things (IoMT) by offering daily cardiovascular monitoring in fragile or pathological individuals, telemedicine solutions, and remote follow-up, thereby opening avenues for new PWV applications.

Supporting Information

Supporting Information is available from the Wiley Online Library or from the author.

Acknowledgements

The authors acknowledge the financial support from the European Union through the ERC project SUPRA2DMAT (GA-833707) and the HORIZON-EIC-2023-PATHFINDEROPEN-01-01 project HYPERSONIC (GA-101129613) as well as the ANR through the Interdisciplinary Thematic Institute SysChem via the IdEx Unistra (ANR-10-IDEX-0002) within the program Investissement d'Avenir, the Foundation Jean-Marie Lehn and the Institut Universitaire de France (IUF).

Conflict of Interest

The authors declare no conflict of interest.

Data Availability Statement

The data that support the findings of this study are available from the corresponding author upon reasonable request.

Keywords

cardiovascular monitoring, graphene, healthcare, pressure sensor, pulse wave velocity

Received: June 3, 2024
Revised: September 23, 2024
Published online: October 10, 2024

- [1] S. Mendis, I. Graham, J. Narula, *Glob Heart* **2022**, *17*, 48.
[2] R. A. Xuereb, C. J. Magri, R. G. Xuereb, *Curr. Cardiol. Rep.* **2023**, *25*, 1337.
[3] C. Chi, Y. Liu, Y. Xu, D. Xu, *Front. Cardiovasc. Med.* **2021**, *8*, 707162.
[4] G. Fiori, F. Fuiano, A. Scorza, S. Conforto, S. A. Sciuto, *R-BME* **2022**, *15*, 169.

- [5] T. T. van Sloten, M. T. Schram, K. van den Hurk, J. M. Dekker, G. Nijpels, R. M. A. Henry, C. D. A. Stehouwer, *J. Am. Coll. Cardiol.* **2014**, *63*, 1739.
[6] Y. C. Chiu, P. W. Arand, S. G. Shroff, T. Feldman, J. D. Carroll, *Am. Heart J.* **1991**, *121*, 1460.
[7] A. Valerio, I. Buraïoli, A. Sanginario, G. Mingrone, D. Leone, A. Milan, D. Demarchi, *Biomed. Signal Process. Control.* **2024**, *93*, 106161.
[8] P. Boutouyrie, M. Briet, C. Collin, S. Vermeersch, B. Pannier, *Artery Res.* **2008**, *3*, 3.
[9] M. J. van Hout, I. A. Dekkers, J. J. Westenberg, M. J. Schalijs, R. L. Widya, R. de Mutsert, F. R. Rosendaal, A. de Roos, J. W. Jukema, A. J. Scholte, H. J. Lamb, *J. Cardiovasc. Magn. Reson.* **2021**, *23*, 46.
[10] G. Mancia, R. Kreutz, M. Brunström, M. Burnier, G. Grassi, A. Januszewicz, M. L. Muiesan, K. Tsioufis, E. Agabiti-Rosei, E. A. E. Algharably, M. Azizi, A. Benetos, C. Borghi, J. B. Hitij, R. Cifkova, A. Coca, V. Cornelissen, J. K. Cruickshank, P. G. Cunha, A. H. J. Danser, R. M. de Pinho, C. Delles, A. F. Dominiczak, M. Dorobantu, M. Dumas, M. S. Fernández-Alfonso, J.-M. Halimi, Z. Járαι, B. Jelaković, J. Jordan, et al., *J. Hypertens.* **2023**, *41*, 1874.
[11] I. Buraïoli, D. Lena, A. Sanginario, D. Leone, G. Mingrone, A. Milan, D. Demarchi, *IEEE Trans. Biomed. Circuits Syst.* **2021**, *15*, 133.
[12] I. Buraïoli, D. Demarchi, A. Milan, F. Veglio, D. Leone, F. Vallelonga, EP4247245A1, **2023**.
[13] M. Butlin, A. Qasem, *Pulse* **2017**, *4*, 180.
[14] S. Conoci, F. Rundo, G. Fallica, D. Lena, I. Buraïoli, D. Demarchi, presented at *IEEE Biomedical Circuits and Systems Conference (BioCAS)*, Cleveland, OH, USA, **2018**.
[15] P. Fallica, D. Lena, F. Rundo, S. Conoci, *Sensors and Microsystems*, Springer, Cham **2022**, vol 918, 314.
[16] A. Sanginario, I. Buraïoli, M. Pogliano, P. Natale, D. Leone, G. Mingrone, A. Milan, D. Demarchi, presented at *IEEE International Symposium on Circuits and Systems (ISCAS)*, IEEE, Montesrey, CA, USA, **2023**, pp. 1–1.
[17] P. Mao, H. Li, Z. Yu, *Sensors* **2023**, *23*, 3673.
[18] X. Wang, Z. Liu, T. Zhang, *Small* **2017**, *13*, 1602790.
[19] S. Sharma, A. Chhetry, M. Sharifuzzaman, H. Yoon, J. Y. Park, *ACS Appl. Mater. Interfaces* **2020**, *12*, 22212.
[20] X. Wang, Z. Feng, Y. Xia, G. Zhang, L. Wang, L. Chen, Y. Wu, J. Yang, Z. L. Wang, *Nano Energy* **2022**, *102*, 107710.
[21] A. K. Bijender, *Sens. BioSensing Res.* **2021**, *33*, 100434.
[22] W. Liu, J. Cheng, Z. Wu, J. Li, W. Shi, W. Yang, N. Jin, Y. Mu, B. Weng, J. Wu, D. Hao, C. Liu, Z. Wang, G. Li, L. Dong, *IEEE Sens. J.* **2022**, *22*, 19818.
[23] Y. Pang, K. Zhang, Z. Yang, S. Jiang, Z. Ju, Y. Li, X. Wang, D. Wang, M. Jian, Y. Zhang, R. Liang, H. Tian, Y. Yang, T.-L. Ren, *ACS Nano* **2018**, *12*, 2346.
[24] L. Chen, M. Lu, H. Yang, J. R. Salas Avila, B. Shi, L. Ren, G. Wei, X. Liu, W. Yin, *ACS Nano* **2020**, *14*, 8191.
[25] Y. Yang, W. Gao, *Chem. Soc. Rev.* **2019**, *48*, 1465.
[26] C.-B. Huang, S. Witomska, A. Aliprandi, M.-A. Stoeckel, M. Bonini, A. Ciesielski, P. Samorł, *Adv. Mater.* **2019**, *31*, 1804600.
[27] S. Vitale, H. Puozzo, S. Saiev, L. Bonnaud, A. G. Ricciardulli, A. Ciesielski, D. Beljonne, P. Samorł, *Chem. Mater.* **2023**, *35*, 6909.
[28] I. B. Wilkinson, C. M. McEniery, G. Schillaci, P. Boutouyrie, P. Segers, A. Donald, P. J. Chowienczyk, *Artery Res.* **2010**, *4*, 34.